═══ **WATER TREATMENT AND DEMINERALIZATION TECHNOLOGY** ═══

Preparation, Characterization of Zirconium Phosphate Composites and Their Adsorption Properties of Phenolic Wastewater

Xue-Li Liu[a, b, *], Si-Jin Li[a], Ya-Li Sun[a], and Lan-Lan Wang[a]

[a] College of Material and Chemical Engineering, Chuzhou University, Anhui, 239012 China
[b] School of Chemistry and Chemical Engineering, AnHui University, HeFei, 230601 China
* e-mail: n_xueli@163.com, n_xueli@chzu.edu.cn

Abstract—In this study, a series of organic amine-intercalated α-ZrP were prepared. The crystal phase, structures and properties of these intercalated compounds were analyzed and characterized using several analysis methods. The interlayer distance of organic amine-intercalated α-ZrP has increased regularly along with the increase of chain elongation of organic amine. The composites were applied to adsorb phenol from wastewater. The adsorption equilibrium, kinetics, and dynamic adsorption of phenol onto intercalated α-ZrP were studied. Adsorption isotherms of phenol were determined at different temperatures, and they were well fitted to the Freundlich equation ($R^2 > 0.99$), and the corresponding maximum adsorption capacity of phenol was 0.832 mmol/g. Batch kinetic experiments revealed that the adsorption process followed a quasi-second-order kinetic model. The dynamic adsorption revealed that the adsorption capacity for phenol increased with the increase in temperature. The adsorption process was rapid and equilibrium was reached within 30 min. When the adsorption dosage is 0.1 g/15 mL, the adsorption yield for 10 mmol/L phenol solution can reach 61.2%.

INTRODUCTION

Nowadays water resources preservation by preventing their pollution by toxic elements is one of the most important challenges for the humans, and it has been noted that surface water and groundwater resources were polluted by several different inorganic-organic chemicals, for example, dyes, pesticides, volatile phenolic compounds, and toxic heavy metal ions [1, 2]. Therefore, even at the lower concentration, the existence of phenolic compounds in discharged water represents a serious problem because of their toxicity and harmfulness to living organisms [3, 4]. Consequently, the treatment of these effluents before their discharge into receiving waters is essential. There are several approaches to removing the phenols from water and wastewater, for example, extraction, distillation, precipitation, membrane separation processes, adsorption, chemical oxidation, etc. [5, 6]. Due to the economic, ecological, and technological advantages, the adsorption method has received considerable attention for the past few years. There are several adsorbents could be employed, e.g. clay and natural mineral adsorbents, polymer-based adsorbents, and novel adsorbents [7].

As a new type of multi-functional inorganic material, zirconium phosphates (ZrP) are widely used in several different chemical fields, including ion exchange, thermostability, adsorption, catalysis, and acid-base resistance properties [8−10]. Compared to amorphous ZrP, the crystalline ZrP ($Zr(HPO_4)_2 \cdot 2H_2O$, hereafter α-ZrP) with a layered structure has attracted more attention substantially because of its ease of structure control, excellent exfoliation, and intercalation properties which leading to design and synthesis new functional materials that fulfil stated requirements [8]. The α-ZrP materials have been used as a new adsorbent material for the removal of heavy metal and dye water pollutants [10]. In recent years, the preparation of a variety of intercalation compounds with new functions has been a hot field in inorganic-organic hybrid materials research. For the pure host α-ZrP, there was virtually no absorption of the phenols [11−13]. A series of the organic amine intercalated α-ZrP compounds which can be synthesized by the interaction with various amino-group or imino-group compounds between layers and layers of α-ZrP,

has attracted much interest. An earlier study by Tsuhako in 2003 was directed toward the adsorption of phenols by butylamine-(C₄N) and octylamine-(C₈N) intercalated α-ZrP. The results indicated that the maximum adsorption was associated with the insertion quantity of alkylamine and the void space in the interlayer region of the host α-ZrP [11]. More recently, a new range of surfactant intercalated α-ZrP with trimethyl quaternary ammonium salts of dodecyl-, tetradecyl-, hexadecyl- and stearyl- was synthesized by Chen, which have good adsorption performance on phenols in water [12, 13].

It is well-known that adsorption thermodynamics and kinetics are important issues of adsorption separation research. It provided the fundamental data used in the following recovery process design [14, 15]. Despite vast studies on synthesis, characterization, and adsorption mechanism for phenols of intercalated α-ZrP compounds, there are relatively few studies focusing on factors that influence the process of phenol uptake and the removal of phenol in dynamics mode. In this article, the synthesis of organic amine-intercalated α-ZrP is demonstrated. Diversified characterizations were studied, the adsorption ability for phenol was also investigated, and the conditions for adsorption, such as temperature, contact time and initial concentration, were comprehensively assessed. The adsorption equilibrium, kinetics, and dynamic adsorption process of phenol onto intercalated α-ZrP compounds were studied. Kinetic and thermodynamic parameters were determined, and the adsorption thermodynamics and kinetics models were concretely evaluated.

EXPERIMENTAL

Materials

α-ZrP made by our laboratory [13], Methylamine (40 wt %, H₂O), triethylamine, triethanolamine, 3-(dimethyl amino)-1-propylamine, *n*-butylamine were analytical grade, phenol from Energy Chemical. The deionized water was used throughout all the experiments.

Preparation of Intercalated α-ZrP Compounds

α-ZrP was intercalated by amines with the stoichiometric mass ratio of 2 : 1 (amines to α-ZrP). Before intercalation, each sample of α-ZrP (0.6 g) was pre-dispersed in 20 mL of deionized water for 0.5 h and dispersed homogeneously by electromagnetic stirring. Next, the intercalating agent was diluted in deionized water and dropped to the α-ZrP suspension slowly following the ratio of solid to liquid of 100 mL/g, and then, stirred for 12 h at room temperature, separated by centrifugation, washed, then dried at 60°C. Finally, the products were recorded as M-ZrP (methylamine intercalated), E-ZrP (triethylamine intercalated), B-ZrP (*n*-butylamine intercalated), H-ZrP (*n*-hexylamine intercalated), O-ZrP (*n*-octylamine intercalated), D-ZrP (*n*-dodecylamine intercalated).

Characterization

The X-ray diffraction patterns were tested with a Bruker X-ray diffractometer (D8 Advance) and CuK_α radiation detector. The scanning electron microscopy (SEM) images were measured by a JSM-6510LV ultra-scanning electron microscope (Jeol, Japan). A Nicolet 6700 FTIR spectrometer was used to identify the surface functional groups in the wavenumber ranging from 400 to 4000 cm⁻¹. The UV-visible absorption data of the adsorption experiment was measured by a spectrophotometer (Varian Cary 100, Varian Corp., United States).

Preparation of Phenol Solution and Content Calibration by UV Spectrophotometry

The solution of phenol standard in water to contain 100 mmol/L was prepared. 0.1, 0.2, 0.3, 0.4, 0.5, 0.6, 0.7, and 0.8 mL of the standard solution were transferred to a 100 mL volumetric flask and diluted each to scale with deionized water. The maximum absorption peak for phenol was observed at 270 nm by a scan of the sample in the range 700−200 nm. The calibration curves for phenol ranging in concentration from 0 to 1 mmol/L were obtained, and the data constructed for the standards gave a linear calibration curve that obeyed the Beer−Lambert law with a correlation coefficient of 0.9997 (Fig. 1). The assays were performed in replicate ($n = 3$) and blank tests were realized. After the analysis of the calibration curve, we got an equation as follows:

$$Y = 1.446X + 0.0141, \quad r = 0.9997. \tag{1}$$

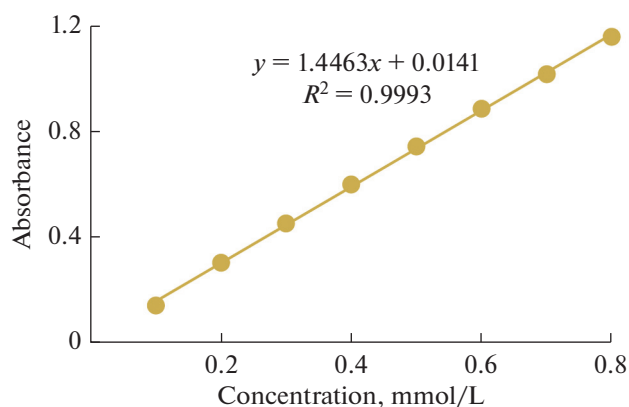$$y = 1.4463x + 0.0141$$
$$R^2 = 0.9993$$

Fig. 1. The linear curve of reference substance of phenol.

The relative standard deviation (RSD) denoting the repeatability of this method is 0.55% ($n = 6$), which manifests that the method is precise enough.

Adsorption Experiment

Adsorption equilibrium experiment. Each intercalation compound was accurately weighted (0.1000 g), and added to standard phenol solutions (15.00 mL, 10 mmol/L), and the flasks were stirred for 6 h, achieved adsorption equilibrium, and then separated by centrifugation. The absorbance of the supernatant was measured, and the precipitate residue dried at 60°C after washing immediately. The control experiment was carried out with the original α-ZrP at the same condition. The maximum amount of adsorbed phenol (Q_e, mmol/g) can be calculated:

$$Q_e = \frac{(C_0 - C_e)V}{m}. \tag{2}$$

The values C_0 and C_e represent the initial and equilibrium concentration of phenol (mmol/L), V is the volume of phenol solution (L), and m is the mass of the ZrP adsorbent (g).

Adsorption thermodynamic experiment. Isotherms comprise an essential part of adsorption studies. From them, it is possible to evaluate the physical interactions between adsorbate and adsorbent. The experimental curves were obtained in 15 mL phenol solutions with concentrations of 1, 3, 5, 7, 10, 15, and 20 mmol/L at 293.15, 308.15, and 323.15 K for 6 h. Samples were filtered and analyzed.

Adsorption kinetics experiment. A kinetics study provides information like reaction order and rate constants, important factors to apply the adsorption process. In these experiments, contact time varied between 0 and 90 min, until equilibrium was observed. The concentration tests remained at 1, 5, and 10 mmol/L, respectively. The temperatures were also kept as 293.15, 308.15, and 323.15 K.

RESULTS AND DISCUSSION

Physicochemical Characterization

X-ray diffraction pattern. Figures 2 and 3 depict the structure and crystal phase of α-ZrP and different organic amine intercalated α-ZrP compounds, we discovered that the layered structures remained after intercalation; this is also consistent with the SEM appearance (Fig. 4). As shown in Fig. 1, the distance of lamellar structure of different organic amine intercalated α-ZrP compounds increase dramatically when compared with pure α-ZrP (7.6 Å) [16, 17]. The distance of lamellar structure of M-ZrP and E-ZrP are only 1.2 and 1.25 nm, and the maximum layer spacing of B-ZrP, H-ZrP, O-ZrP and D-ZrP are 1.82, 2.22, 2.67, and 1.78 nm, respectively, which is a connection with the chain lengths of alkyl groups in different intercalated organic amine. Remarkably, the spacing of layers has increased regularly along with the increase of chain elongation of organic amine. With a rise in the number of carbon atoms, the change of interplanar distances has regularity. For example, $\Delta((n8-n6)/2) = 0.22$ nm, $\Delta((n6-n4)/2) = 0.20$ nm and $\Delta((n4-n1)/3) = 0.21$ nm. So obviously, there is sort of a straight-line relationship here. By linear regression, the linear relationship between the spacing of layers and the number of carbon atoms of amines was obtained, i.e., $d = 0.209n + 0.9887$, $r = 0.9998$, where d (nm) and n ($n = 1, 4, 6, 8$) in equation equal the
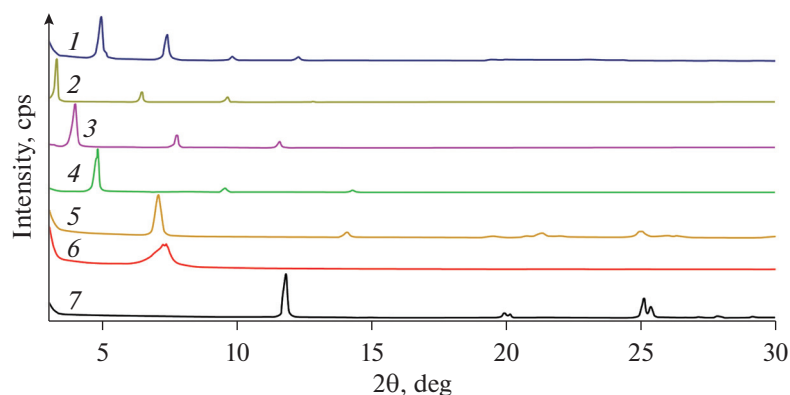
Fig. 2. The XRD patterns of the intercalation compounds and α-ZrP: (*1*) 1.78 (D-ZrP), (*2*) 2.67 (O-ZrP), (*3*) 2.22 (H-ZrP), (*4*) 1.82 (B-ZrP), (*5*) 1.25 (E-ZrP), (*6*) 1.20 (M-ZrP), (*7*) 0.76 nm (α-ZrP).
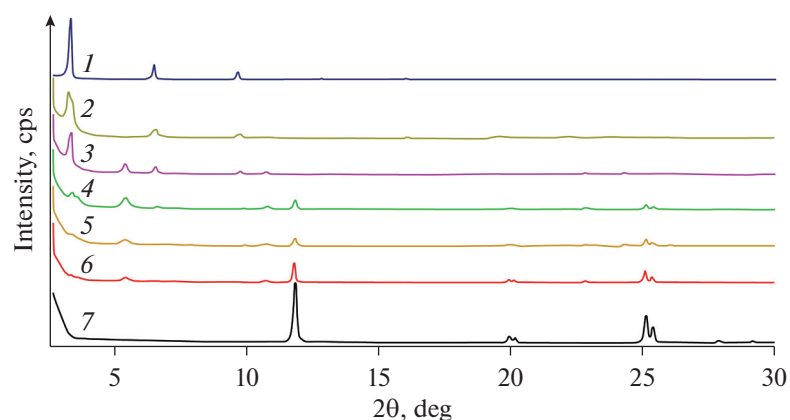

Fig. 3. The XRD patterns of the O-ZrP with different molar ratios of amine to α-ZrP: (*1*) 4.6 : 1 (2.67 nm), (*2*) 2 : 1 (2.70 nm), (*3*) 1.5 : 1 (2.67 nm), (*4*) 1 : 1, (*5*) 0.7 : 1, (*6*) 0.5 : 1, (*7*) α-ZrP.

interlayer spacing and the number of carbon atoms in the corresponding alkyl chain. This illustrates that the whole amine molecular is almost perpendicular to the layer [18], after all, the molecular length is reckoned at 0.216 nm for every −CH$_2$ increase in an organic amine. By contrast, we found the original XRD diffraction at $2\theta = 11.65°$ disappeared, which indicated that the different organic amines were intercalated into the interlayer space of α-ZrP successively. All the x-ray diffraction patterns are sharp and regular, and these results demonstrate convincingly that all the α-ZrP compounds have higher crystallinity and pure phase. In addition, it is too difficult to be intercalated into the galleries of α-ZrP directly for n-dodecyl amine by the reason of the spatial configuration of the larger molecular with a long-chain alkyl group structure. So, it is quite necessary to weaken and break up the interactions of α-ZrP laminate by using the colloidization agent [19]. All up, the O-ZrP was selected as the subject in laboratory experiments.

As exhibited in Fig. 3, the interlayer distances of O-ZrP are pretty much the same with n(octyl-amine)/n(α-ZrP) within the scope of 0.5−1.0. The interlamellar spacing increases with the increasing of the intercalation ratio of n-octylamine to α-ZrP. The interlayer distances would be more than 2.67 nm for any value of n(octylamine)/n(α-ZrP) greater than 1.5. Meanwhile, the diffraction peaks for O-ZrP are at 3.30°, 6.45°, and 9.63° (2θ), respectively. Thereinto, the sharpest and strongest peak appears at a small 2θ angle (3.30°), signifying a large d value (interlayer distance) is obtained, which is calculated to be 26.7 Å according to the Bragg equation. The former two diffraction peaks are also sensitively and intensely, suggesting that it is an ordered collection of the n-octylamine molecules between the sheets of layered zirconium phosphate [20]. This phenomenon has led to the form of a single-phase intercalation compound, and the d-spacing continuously increases along with more intercalating molecules until saturation [16]. To sum up, the prepared O-ZrP compound is highly crystallized with a maximum interlayer distance of 26.7 Å, and the molar ratio of n-octylamine to α-ZrP in the intercalation composite was selected to be 1.5 : 1.
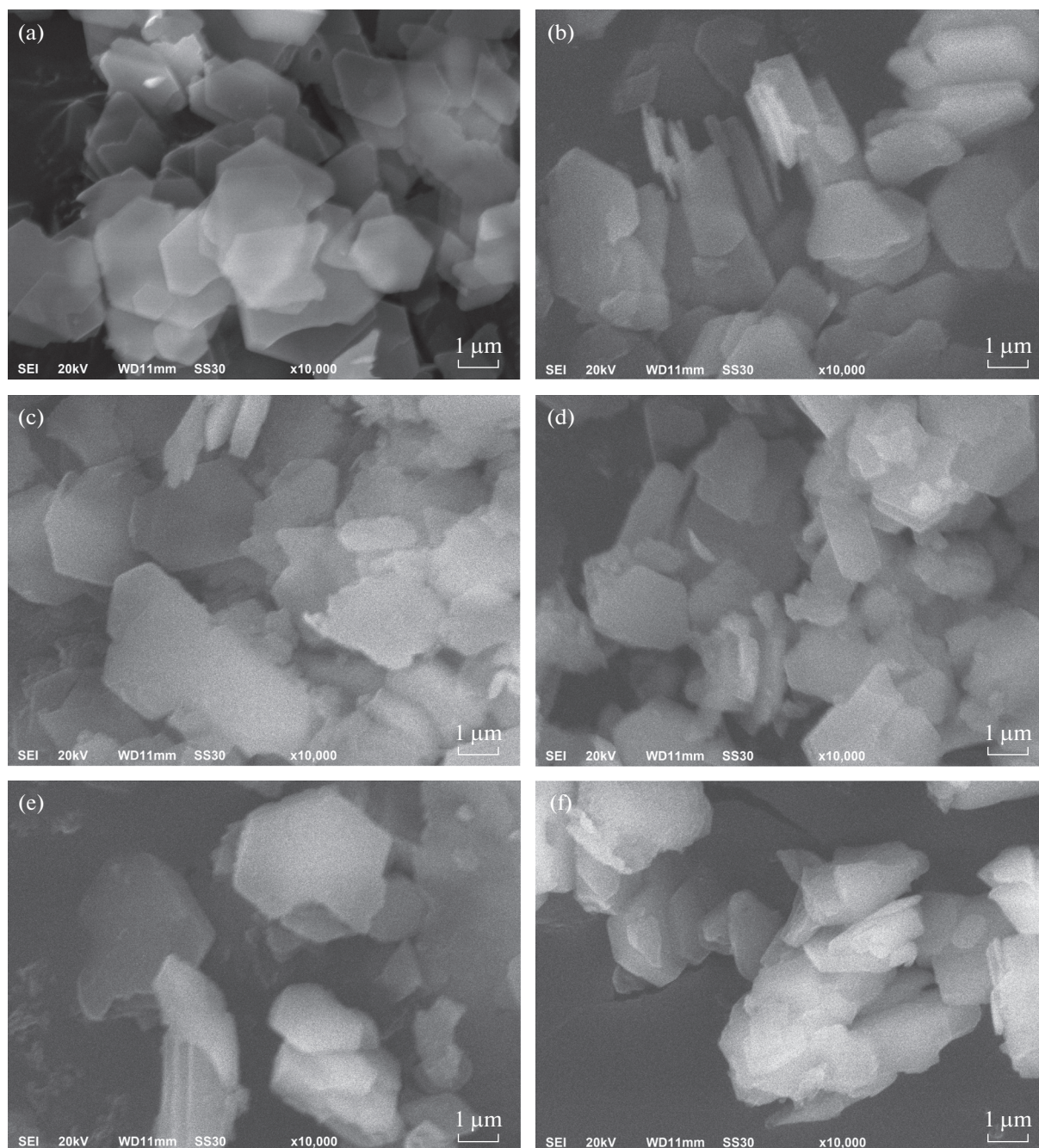
Fig. 4. SEM images for α-ZrP (a) and O-ZrP with different mole ratios: (b) 0.5 : 1; (c) 0.7 : 1; (d) 1.0 : 1; (e) 1.5 : 1; (f) 2.0 : 1.

SEM of α-ZrP and intercalated α-ZrP compounds. α-ZrP is a typical layered material. As shown in Fig. 4a, the α-ZrP exhibit a perfect layered structure and less regularly hexagonal shape and the largest nanoplatelet has a sheet structure with lateral dimensions of about 500 nm. The morphologies of the prepared O-ZrP are also shown in Figs. 4b−4f. With the ratio of n(octylamine)/n(α-ZrP) increasing to 0.5−2.0, the original lamellar hexagonal plates were covered with n-octylamine. As a result, there are only a few areas where you can see the exposed hexagonal plates. However, it is glaringly obvious that the O-ZrP sample is a lamellar and the sheet morphology of α-ZrP remains after intercalation, which is analogous to the morphology of α-ZrP. As you can see in the above figures, the lateral dimension of the composite materials can be achieved in approximately 1.3−1.5 μm.
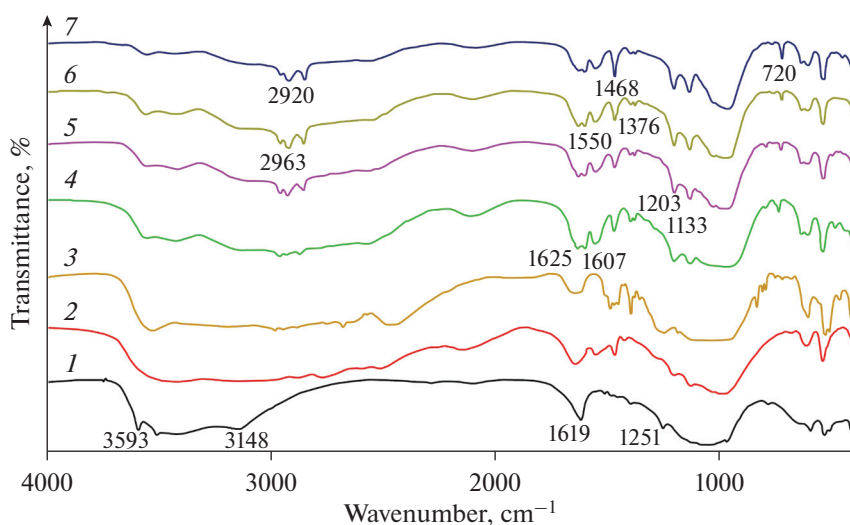
Fig. 5. FTIR spectra of (*1*) α-ZrP and O-ZrP with different mole ratios: (*2*) 0.5 : 1; (*3*) 0.7 : 1; (*4*) 1.0 : 1; (*5*) 1.5 : 1; (*6*) 2.0 : 1; (*7*) 4.6 : 1.

FTIR spectroscopy. The FTIR spectra of the samples are displayed in Fig. 5. For α-ZrP (Fig. 5a), the peaks of 3593 and 3510 cm^{-1} pertain to the antisymmetric stretching vibration of interlayer crystalline water, and peaks of 3150 and 1619 cm^{-1} are attributable to the symmetric stretching vibration and bending vibration of water. The peak at 1251 cm^{-1} is bound to the stretch of the P−OH bond within the interlayer of α-ZrP, which is also the characteristic peak of the HPO_4^{2-} group. In the range of 1200−1000 cm^{-1} showed stretching vibration absorption for the P−O bond. Figures 5b−5g is the IR spectrum of six *n*-octylamine intercalated α-ZrP with the molar ratio of *n*(octylamine)/*n*(α-ZrP) in the range of 0.5−4.6. After *n*-octylamine was intercalated into α-ZrP, the intensity of the peaks and the absorption bands from 3600 to 3500 cm^{-1} corresponding to the crystallization water were weakened and even almost disappeared. And secondly, from Fig. 5, you can see that the IR spectra peaks not just shifted to lower wave numbers direction, but also became wider. It's been signalling that most of the crystalline water was precluded by *n*-octylamine. The IR spectrums of six *n*-octylamine intercalated α-ZrP were similar. All the absorption peaks located at 2963, 2920, 2850, 1625, 1607, 1550, 1468, 1376, 1203, 1133 and 720 cm^{-1} are somewhere to the characteristic peaks of O-ZrP. Among them, two peaks at 2963 and 2920 cm^{-1} correspond to the asymmetric stretching vibration of −CH$_3$ and −CH$_2$− of the octyl group. The peak toward 2850 cm^{-1} was attributed to the C−H stretching vibration. The new peaks of 1468 and 1376 cm^{-1} belong to the bending vibration of the C−H bond. The peak of 720 cm^{-1} belongs to the rocking vibration of −(CH$_2$)$_n$-bond. In addition, the peaks of 1203 and 1133 cm^{-1} are assigned to the stretching vibration of the C−N bond and the absorption of the N−H bending vibration was observed at 1607 cm^{-1}. Beyond that, both the peaks at 1625 and 1607 cm^{-1} are related to the bending vibration of NH_3^+, and all of them prove that the intercalated *n*-octylamine molecule is combined with HPO_4^{2-} by ionic bond (O$_3$P−O$^-$H$^+$NH$_2$C$_8$H$_{17}$). Moreover, the characteristic peak intensity of the HPO_4^{2-} group (1251 cm^{-1}) has been weakened after intercalation. All the results reveal that *n*-octylamine has been successfully intercalated into the α-ZrP, and the conclusion brings into correspondence with the XRD results.

Phenolic Compounds Adsorption Performance of α-ZrP Intercalation

The absorption effect of O-ZrP with the different insert amounts of *n*-octylamine. Figure 6 shows the relationship between the absorption amount (Q_e) of phenol and the insert amount (*C*) of *n*-octylamine in α-ZrP. With the increase in *n*(octylamine)/*n*(α-ZrP), the adsorption performance of phenol of O-ZrP went up first but then it went down, i.e., the Q_e of phenol increased with the increase of *C* up to 1.5 but decreased above it. By now the maximum adsorption capacity can reach 0.82 mmol/g. Hereafter, the Q_e of phenol descended with time and tended to be stable. It is widely known that both spacing between the
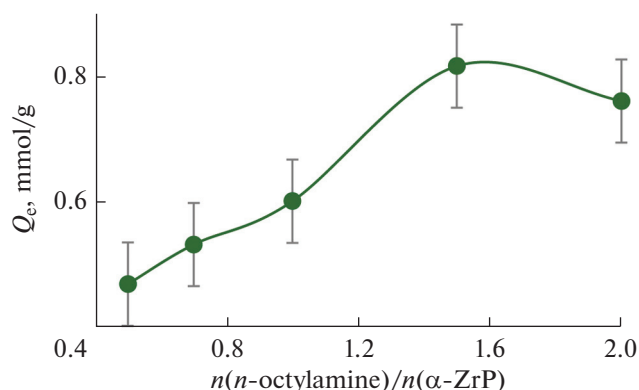
Fig. 6. The absorption amount (Q_e) of phenol of O-ZrP and the insert amount (C) of *n*-octylamine.

layers, the acidity regulation and hydrophobicity of the alkyl chain are crucial for the adsorption of phenol by alkylamine-intercalated α-ZrP [11]. The HPO_4^{2-} group of α-ZrP is completely neutralized by excess n-octylamine. Meanwhile, the octylamine in the interlayer region is arranged tightly, and this can result in lacking enough void space [13].

The isotherm adsorption models. Here are three sorption isotherm models, Linear, Freundlich and Langmuir isotherm models, which were chosen to simulate and evaluate the relationship between the Q_e and C_e in aqueous solution. The Linear isotherm model, Freundlich model and Langmuir isotherm model can be presented as (3), (4) and (5), respectively [21].

$$Q_e = K_l C_e + b, \tag{3}$$

$$Q_e = K_F C_e^{1/n}, \tag{4}$$

$$\frac{C_e}{Q_e} = \frac{1}{K_L q_m} + \frac{C_e}{q_m}, \tag{5}$$

where K_l (L/g) is the partition coefficient; b, K_F (L/g) and K_L (L/g) are the partition constant; n is the empirical parameter; q_m (mmol/g) is the Langmuir constant related to the maximum monolayer adsorption capacity.

Effect of temperature on phenol adsorption isotherm. The effects of varying intercalation compound concentration and the temperature (293.15, 308.15, 323.15 K) on the removal of phenol from aqueous solutions were investigated by using initial phenol concentrations of 1.0, 3.0, 5.0, 7.0, 10.0, 15.0, and 20.0 mmol/L, respectively. As shown in Fig. 7(a), the adsorption capacity of phenol on O-ZrP increased with the increase in temperature, indicating that the adsorption of phenol on O-ZrP is an endothermic process. Three well-known adsorption models were simulated, and the equilibrium data were obtained and shown in Fig. 7 and Table 1.

With the growth of the temperature, the Q_e of adsorption growth rate has slowed. The adsorption isotherms of phenol onto O-ZrP exist in certain linear over a wide range C_0 of 1.0–20.0 mmol/L, and the Freundlich and the Langmuir models can be selected to fit the data. As to 293.15 K, the adsorption isotherm of phenol is linear over a wide range C_0 of 1.0–15.0 mmol/L, but it will turn nonlinear when $C_0 >$ 15.0 mmol/L. Furthermore, the adsorption isotherm of the Langmuir model has higher fitting degrees at normal temperature, and the coefficient of determination ($R^2 = 0.9985$) in the Langmuir model was closer to 1. With the increase of temperature, i.e., regarding 308.15 and 323.15 K, the adsorption isotherms of phenol change to linear when $C_0 > 5.0$ mmol/L. All things considered, the Freundlich model could better describe the adsorption isotherm of O-ZrP over a wide range C_0 of 1.0–20.0 mmol/L under the higher temperature condition. As can be seen in Table 1, judging from the constant of K_F, raising the temperature can promote the adsorption capacity of O-ZrP. The value of the Freundlich index $1/n$ is less than 1 at different temperatures, indicating a preferential adsorption process, especially at high temperatures. In other words, the increase of the Q_e as a function of the temperature showed the adsorption process was endothermic [22]. This result was consistent with the Freundlich kinetics behaviour of phenol adsorption on O-ZrP at 323.15 K ($1/n < 0.5$).
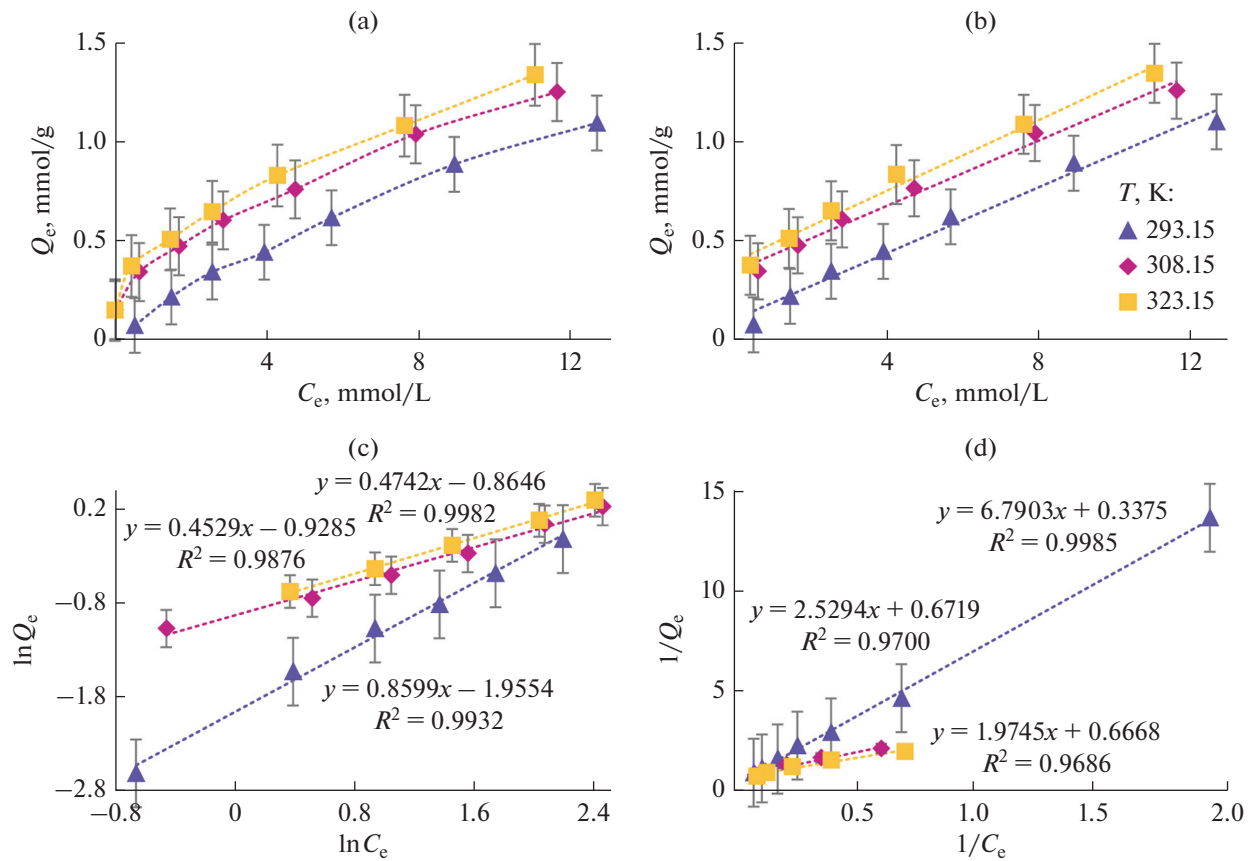
Fig. 7. (a) Effect of initial concentration on adsorption and (b) linear, (c) Freundlich, (d) Langmuir equilibrium isotherms of phenol onto O-ZrP at different temperatures.

The dynamic adsorption models. Adsorption kinetics of phenol onto O-ZrP was executed at initial concentration with 10 mmol/L dosage at 293.15, 308.15 and 323.15 K. As shown in Fig. 8a, the adsorptive capacity increases rapidly with time during the initial phases and reaches a plateau as the contact time increases further. The absorption equilibrium is achieved after only 30 min, and the adsorption capacity is 0.619 (293.15 K), 0.762 (308.15 K) and 0.832 mmol/g (323.15 K), respectively. To research the adsorp-

Table 1. Equilibrium parameters for adsorption of phenol onto O-ZrP

Model	Temperature, K	C_0, mmol/L	Equation	$K_i^{\text{a)}}$	R^2
Linear	293.15	1–15	$Q_e = 0.0943C_e + 0.0688$	0.0943	0.991
	308.15	3–15	$Q_e = 0.0941C_e + 0.3109$	0.0941	0.9943
	323.15	5–20	$Q_e = 0.0943C_e + 0.4268$	0.0849	0.9908
Freundlich	293.15	1–15	$Q_e = 0.1415C_e^{0.8599}$	0.1415	0.9932
	308.15	3–20	$Q_e = 0.3951C_e^{0.4529}$	0.3951	0.9876
	323.15	5–20	$Q_e = 0.4212C_e^{0.4742}$	0.4212	0.9982
Langmuir	293.15	1–20	$1/Q_e = 0.3375 + 6.7903/C_e$	0.0497	0.9985
	308.15	5–20	$1/Q_e = 0.6719 + 2.5294/C_e$	0.2656	0.97
	323.15	5–20	$1/Q_e = 0.6668 + 1.9745/C_e$	0.3377	0.9686

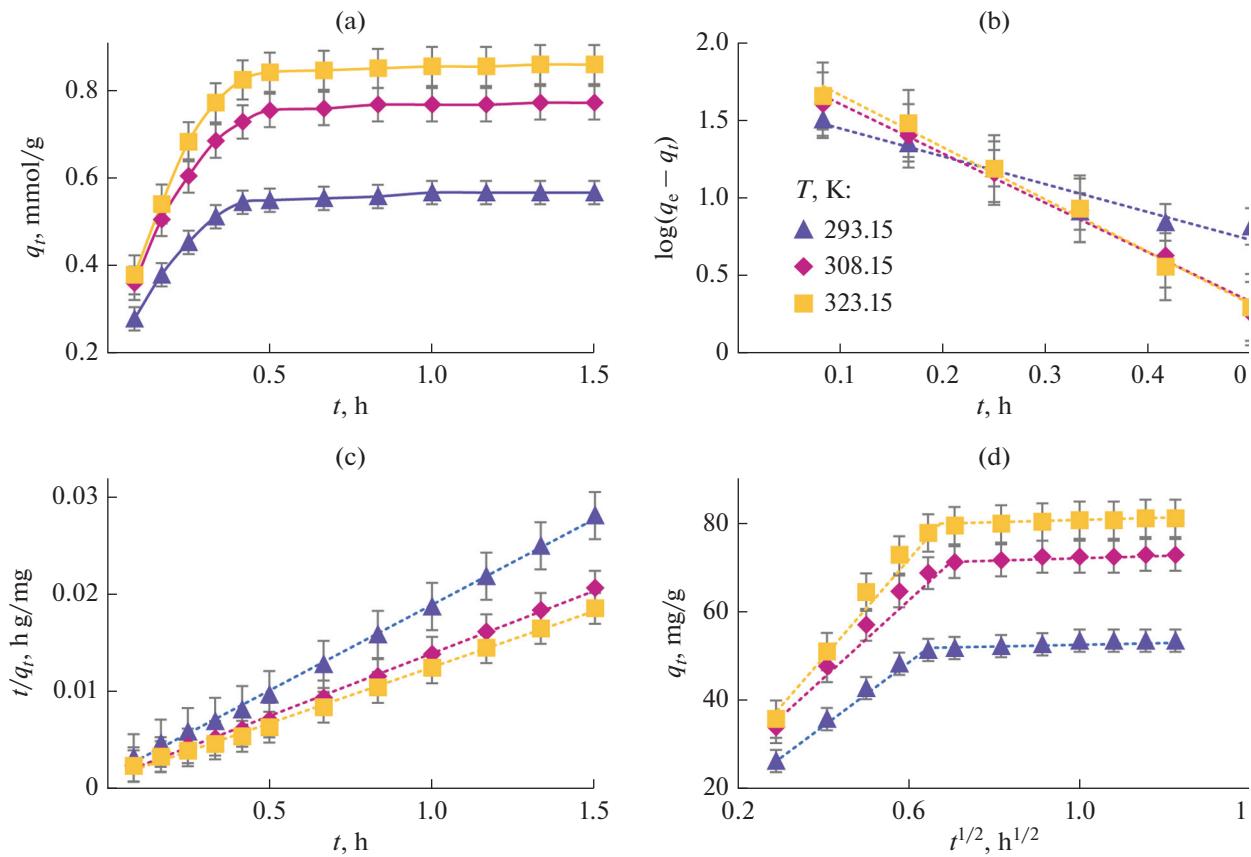a) K_i is the K_l, K_F and K_L respectively.

Fig. 8. Kinetic curves for phenol adsorption onto O-ZrP at different temperatures (a) through the quasi-first-order (b), quasi-second-order (c), and Weber–Morris (d) models.

tion kinetics better, the kinetic experimental data were guided into the quasi-first order (Eq. (6)) and quasi-second order (Eq. (7)) kinetic models, and the Weber–Morris model (Eq. (8)) [23].

$$\log\left(q_e - q_t\right) = \log q_e - \frac{k_1 t}{2.303}, \tag{6}$$

$$\frac{t}{q_t} = \frac{1}{k_2}\frac{1}{q_e^2} + \frac{t}{q_e}, \tag{7}$$

$$q_t = k_3 t^{\frac{1}{2}} + C, \tag{8}$$

where t (h), k_1 (h^{-1}), k_2 (g/(mg h)) and k_3 (mg/g h$^{1/2}$) are referred to as the contact time and the rate constants of quasi first-order, quasi second-order and diffusion kinetic models, respectively; Q_e and q_t are the adsorption capacity (mg/g) of phenol at equilibrium and the corresponding time.

The associated kinetic parameters of quasi-first order, quasi-second order and Weber–Morris models are represented in Table 2. Compared to the quasi-first-order model, the correlation coefficient ($R^2 >$ 0.99) for the quasi-second-order kinetic model was higher. In addition, the calculated values of adsorption saturation capacity Q_e (Table 2) are closer to the experimental data at the corresponding temperature. Consequently, the quasi-second-order model provides a good explanation for the phenol adsorption process by O-ZrP, and the adsorption of phenol appeared to be controlled by the chemisorption process simultaneously [24]. That is to say, the adsorption process happened via surface exchange reactions at a brisk pace at the early stage. After 30 min, phenol diffused into the O-ZrP network for further interactions [25]. Besides, the plots of the Weber–Morris model were not linear over the whole-time range, indicating that more than one adsorption process and the adsorption process contained both the surface adsorption and intraparticle diffusion which by the presence of micropores in the ZrP compounds [13].

Table 2. Kinetic parameters for phenol adsorption by O-ZrP at various temperatures

Model		293.15 K	308.15 K	323.15 K
Quasi-first order	k_1 (h^{-1})	4.134	7.334	7.753
	Q_e (mg/g)^a	42.550	84.256	100.415
	R^2	0.9431	0.9886	0.9918
Quasi-second order	k_2 (g/(mg h))	0.2456	0.1889	0.1688
	Q_e (mg/g)^a	56.497	77.519	86.207
	R^2	0.9983	0.9979	0.9973
Weber–Morris	k_3 (mg/g h$^{1/2}$)	71.302	98.464	120.5
	C	6.2737	6.5775	1.8454
	R^2	0.9936	0.9913	0.9902

* Q_e is the adsorption quantity of the calculative value; the experimental values of Q_e at 293.15, 308.15, and 323.15 K are 58.25, 72.75 and 81.12 mg/g, respectively.

Table 3. Comparison of the adsorption capacity for various adsorbents in phenol removal

Adsorbents	Q_e, mg/g	Ref.
Commercial activated carbon	32	[26]
Crab shell chitosan	190	[27]
Activated clay	5.84	[22]
HDTMA-montmorillonite	94.9	[28]
CTAB-ZrP	84.7	[13]
Butylamine-intercalated α-ZrP	47.06	[11]
O-ZrP	81.12	This work

COMPARISON

Table 3 presents the absorption capacities of phenol on some adsorbents in the literature. In addition, all the units have been standardized and converted to mg/g. As compared with other adsorbents, the Q_e of O-ZrP in this work was higher at 81.12 mg/g. Hence, the ease and availability of ZrP for the synthesis of intercalated α-ZrP, and its adsorption potential made it a promising alternative low-cost adsorbent for phenol removal from wastewater.

CONCLUSIONS

In summary, the intercalation composite of amine-ZrPs has been prepared, and the interlayer distance is expanded from 7.6 to 26.7 Å, which varies with the types and amounts of organic amines. By comparing them, the nonlinear relationship between the spacing of layers and the number of carbon atoms of amines is established. Phenol adsorption by O-ZrP accorded with quasi-second-order and Freundlich models with a maximum adsorption capacity Q_e of 0.832 mmol/g. All these results demonstrated that organic amine-intercalated α-ZrP would place hopes on clearing phenols from wastewater.

CONFLICT OF INTEREST

The authors of this work declare that they have no conflicts of interest.

REFERENCES

1. Rout, P.R., Zhang, T.C., Bhunia, P., and Surampalli, R.Y., Treatment technologies for emerging contaminants in wastewater treatment plants, A review, *Sci. Total Environ.*, 2021, vol. 753, p. 141990.
   https://doi.org/10.1016/j.scitotenv.2020.141990

2. Waheed, A., Baig, N., Ullah, N., and Falath, W., Removal of hazardous dyes, toxic metal ions and organic pollutants from wastewater by using porous hyper-cross-linked polymeric materials: A review of recent advances, *J. Environ. Manage.*, 2021, vol. 287, p. 112360.
   https://doi.org/10.1016/j.jenvman.2021.112360

3. Senturk, H.B., Ozdes, D., Gundogdu, A., Duran, C., and Soylak, M., Removal of phenol from aqueous solutions by adsorption onto organo-modified Tirebolu bentonite: Equilibrium, kinetic and thermodynamic study, *J. Hazard. Mater.*, 2009, vol. 172, no. 1, pp. 353−362.
   https://doi.org/10.1016/j.jhazmat.2009.07.019

4. Park, J.J., and Lee, W.Y., Adsorption, and desorption characteristics of a phenolic compound from Ecklonia cava on macroporous resin, *Food Chem.*, 2021, vol. 338, p. 128150.
   https://doi.org/10.1016/j.foodchem.2020.128150

5. Buscaa, G., Berardinelli, S., Resini, C., and Arrighi, L., Technologies for the removal of phenol from fluid streams: a short review of recent developments, *J. Hazard. Mater.*, 2008, vol. 160, nos. 2−3, pp. 265−288.
   https://doi.org/10.1016/j.jhazmat.2008.03.045

6. Hasan, H.A., Muhammad, M.H., and Ismail, N.L., A review of biological drinking water treatment technologies for contaminants removal from polluted water resources, *J. Water Process Eng.*, 2020, vol. 33, p. 101035.
   https://doi.org/10.1016/j.jwpe.2019.101035

7. Issabayeva, G., Hang, S.Y., Wong, M.C., and Aroua, M.K., A review on the adsorption of phenols from wastewater onto diverse groups of adsorbents, *Rev. Chem. Eng.*, 2018, vol. 34, pp. 855−873.
   https://doi.org/10.1515/revce-2017-0007

8. Xiao, H.P., and Liu, S.H., Zirconium phosphate (ZrP)-based functional materials: Synthesis, properties, and applications, *Mater. Des.*, 2018, vol. 155, pp. 19−35.
   https://doi.org/10.1016/j.matdes.2018.05.041

9. Pica, M., Donnadio, A., and Casciola, M., From microcrystalline to nanosized α-zirconium phosphate: Synthetic approaches and applications of old material with a bright future, *Coord. Chem. Rev.*, 2018, vol. 374, pp. 218-235.
   https://doi.org/10.1016/j.ccr.2018.07.002

10. Pica, M., Treatment of wastewaters with zirconium phosphate based materials: A review on efficient systems for the removal of heavy metal and dye water pollutants, *Molecules*, 2021, vol. 26, no. 8, p. 2392.
    https://doi.org/10.3390/molecules26082392

11. Hayashi, A., Nakayama, H., and Tsuhako, M., Adsorption of phenols by alkylamine-intercalated α-zirconium phosphate, *Bull. Chem. Soc. Jpn.*, 2003, vol. 76, no.12, pp. 2315−2319.
    https://doi.org/10.1246/bcsj.76.2315

12. Yao, W., Wang, H.N., Wang, J.W., Zhong, J., and Chen, R.Y., Preparation, characterization and adsorption mechanism for phenols of CTMAB-ZrP, *Acta Phys-Chim. Sin.*, 2011, vol. 27, no.7, pp. 1763-1771.
    https://doi.org/10.3866/PKU.WHXB20110704

13. Wang, H.N., Liu, W.J., Yao, W., Zhang, K., Zhong, J., and Chen, R.Y., Quaternary ammonium salts intercalated α-ZrP compounds for adsorption of phenolic compounds, *Appl. Surf. Sci.*, 2013, vol. 268, pp. 179−187.
    https://doi.org/10.1016/j.apsusc.2012.12.054

14. Chanajaree, R., Sriuttha, M., Lee, V.S., and Wittayanarakul, K., Thermodynamics, and kinetics of cationic/anionic dyes adsorption on cross-linked chitosan, *J. Mol. Liq.*, 2021, vol. 322, p. 114507.
    https://doi.org/10.1016/j.molliq.2020.114507

15. Vecchio, P.D., Haro, N.K., Souza, F.S., Marcílio, N.R., and Féris, L.A., Ampicillin removal by adsorption onto activated carbon: kinetics, equilibrium, and thermodynamics, *Water Sci. Technol.*, 2019, vol. 79, no. 10, pp. 2013−2021.
    https://doi.org/10.2166/wst.2019.205

16. Sun, L.Y., O'Reilly, J.Y., Kong, D.Y., Su, J.Y., Boo, W.J., Sue, H.J., and Clearfield, A., The effect of guest molecular architecture and host crystallinity upon the mechanism of the intercalation reaction, *J. Colloid Interface Sci.*, 2009, vol. 333, pp. 503−509.
    https://doi.org/10.1016/j.jcis.2009.02.028

17. Cheng, Y., Wang, X.D., Jaenicke, S., and Chuah, G.K., Minimalistic liquid-assisted route to highly crystalline α-zirconium phosphate, *ChemSusChem*, 2017, vol. 10, pp. 3235−3242.
    https://doi.org/10.1002/cssc.201700885

18. Tindwa, R.M., Ellis, D.K., Peng, G.Z., and Clearfield, A., Intercalation of *n*-alkylamines by α-zirconium phosphate, *J. Chem. Soc., Faraday Trans. 1*, 1985, vol. 81, pp. 545−552.

19. Kaschak, D.M., Johnson, S.A., Hooks, D.E., Kim, H.N., Ward, M.D., and Mallouk, T.E., Chemistry on the edge: A microscopic analysis of the intercalation, exfoliation, edge functionalization, and monolayer surface tiling reactions of α-zirconium phosphate, *J Am. Chem. Soc.*, 1998, vol. 120, no. 42, pp. 10887−10894.
https://doi.org/10.1021/ja9818710

20. Chen, R.Y., Yao, W., Wang, H.N., Wang, J.W., and Zhong, J., Synthesis and characterization of tri-*n*-octyl-amine-intercalated α-zirconium phosphate, *Adv. Mater. Res.*, 2011, vol. 284-286, pp. 234−237.
https://doi.org/10.4028/www.scientific.net/AMR.284-286.234

21. Dai, K., Zhang, J., Kou, J.W., Yang, P.P., Li, M., Tang, C.L., Zhuang, W., Ying, H.J., and Wu, J. L., Tunable synthesis of polyethylene polyamine modified lignin and application for efficient adsorption of Fe^{2+} in super acid system, *Sep. Purif. Technol.*, 2021, vol. 272, p. 118950.
https://doi.org/10.1016/j.seppur.2021.118950

22. Dehmani, Y., Sellaoui, L., Alghamdi, Y., Lainé, J., Badawi, M., Amhoud, A., Bonilla-Petriciolet, A., Lamhasni, T., and Abouarnadasse, S., Kinetic, thermodynamic and mechanism study of the adsorption of phenol on Moroccan clay, *J. Mol. Liq.*, 2020, vol. 312, p. 113383.
https://doi.org/10.1016/j.molliq.2020.113383

23. Dai, K., Zhao, G.L., Wang, Z.C., Peng, X.Q., Wu, J.L., Yang, P.P., Li, M., Tang, C.L., Zhuang, W., and Ying, H.J., Novel mesoporous lignin-calcium for efficiently scavenging cationic dyes from dyestuff effluent, *ACS Omega*, 2021, vol. 6, pp. 816−826.
https://doi.org/10.1021/acsomega.0c05401

24. Xie, B.X., Qin, J.H., Wang, S., Li, X., Sun, H., and Chen, W.Q., Adsorption of phenol on commercial activated carbons: Modelling and interpretation, *J. Environ. Res. Public Health*, 2020, vol. 17, p. 789.
https://doi.org/10.3390/ijerph17030789

25. Hao, Z., Wang, C., Yan, Z., Jiang, H., and Xu, H., Magnetic particles modification of coconut shell-derived activated carbon and biochar for effective removal of phenol from water, *Chemosphere*, 2018, vol. 211, pp. 962−969.
https://doi.org/10.1016/j.chemosphere.2018.08.038

26. Stavropoulos, G.G., Samaras, P., and Sakellaropoulos, G.P., Effect of activated carbons modification on porosity, surface structure and phenol adsorption, *J. Hazard. Mater.*, 2008, vol. 151, pp. 414−421.
https://doi.org/10.1016/j.jhazmat.2007.06.005

27. Asokogene, O.F., Muhammad, A.A.Z., Idris, M.M., Surajudeen, A., and Usman, A.E., Adsorption dynamics of phenol by crab shell chitosan, *Int. J Chem. React. Eng.*, 2020, vol. 18, p. 20200014.
https://doi.org/10.1515/ijcre-2020-0014

28. Słomkiewicz, P., Szczepanik, B., and Czaplicka, M., Adsorption of phenol and chlorophenols by hdtma modified halloysite nanotubes, *Materials*, 2020, vol. 13, p. 3309.
https://doi.org/10.3390/ma13153309

Publisher's Note. Allerton Press remains neutral with regard to jurisdictional claims in published maps and institutional affiliations.